ARTICLE

Synthesis, crystallographic study and solid-state properties of metal-free perovskites with P-atom containing A-site cations

Received 00th January 20xx,
Accepted 00th January 20xx

DOI: 10.1039/x0xx00000x

Yumi Matsuda,[a] Rentarou Asai,[a] Jumpei Moriguchi,[a] Tomoyuki Akutagawa,[b] Atsuko Masuya-Suzuki[a] and Ryo Tsunashima*[a]

A P-atom was introduced at the A-site in the metal-free perovskite $A(NH_4)X_3$ using 1,3,5-triaza-7-phosphaadamantane (pta) after the compound had been diprotonated, where X represents Br^-, I^-, and BF_4^- anions, labelled as **p-Br**, **p-I**, and **p-BF_4**, respectively. The pta is analogous to hexamethylenetetramine (hmta) with one N-atom replaced by a P-atom. The **p-Br** and **p-BF_4** perovskites were not isostructural with the corresponding perovskite structure that utilised hexamethylenetetramine (hmta) as the A-site cation. The **p-Br** undergoes a phase transition from order phase to a thermally disordered plastic crystalline phase, whereas hmta-anaogy **h-Br** does not transit to the disordered structure. The decrease in molecular symmetry from hmta to pta was considered the reason for the loss of orientational order. The **p-I** exhibited greenish photoluminescence, in contrast with the orangish photoluminescence observed in the dabco-based metal-free perovskites. Introduction of P-atom at the A-site molecule was found to lead to differencesin phase transition and photoluminescence, providing a new molecular design for metal-free perovskites.

Introduction

Extensive research and development of perovskite compounds have been carried out due to their diverse applications in electric, magnetic, and optical material. Perovskites like $BaTiO_3$ (BTO) and $Pb(Zr, Ti)O_3$, which are traditional inorganic examples, have been utilised in various applications, including capacitors, SONAR systems, speakers, and actuators, due to their ferroelectric and/or piezoelectric properties.[1, 2] In response to growing requirements for energy-efficient, cost-effective, and environmentally sustainable materials, molecular ferroelectrics have garnered substantial interest.[3-7] Among molecular-based ferroelectric materials, the development of the metal-free perovskite structures has emerged as a notable trend in recent years.[7-25]

Metal-free perovskites are an emerging material group. The ferroelectric properties were reported in 2018[7] after a report on their crystal structure in 2002.[8] The spontaneous polarisation of $MDABCO(NH_4)I_3$ (MDABCO = methylated and protonated diazabicyclo[2.2.2]octo) reaches 19 $\mu C/cm^2$, which is comparable to 26 $\mu C/cm^2$ for BTO. Solid-state properties, for example, piezoelectricity, X-ray detection, mechanical property, elastic property, electrocaloric effects, electro-optic property and photo luminescence (PL) have been investigated *via* tailoring and tuning their properties through the design of A-site molecule.[13-23] Solid solutions are also achieved for A-site with spherical molecules towards tuning these solid-state properties like metal-containing perovskites[24]. In addition to the three-dimensional quasi-cubic perovskites, the two-dimensional layered perovskite $A_2B_2X_4$ was also developed.[25]

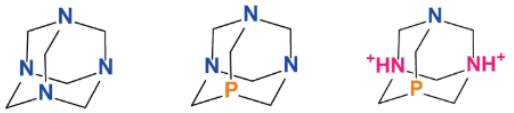

Figure 1. Molecular structure of pta, $ptaH_2^{2+}$ and hmta.

The perovskite is a typical structure for a ternary phases. The structure of the A, B, and X ions is based on the lock-salt-type arrangement of BX, but one $\{BX_6\}$ octahedron is substituted by the A ion. Molecules can also adopt a perovskite structure if they meet the requirements of charge balance and the geometric restriction commonly referred to as the Goldschmidt tolerance factor. A conventional metal-free perovskite has an ABX_3 stoichiometric composition and consists of the divalent cation A^{2+}, which arises from protonation and/or methylation of the N-atom in a cyclic or spherical organic amine. The B-site is composed of either H_3O^+ or NH_4^+, and the X site consists of ions including halide ions, ClO_4^- and BF_4^-.[9-11] Along with NH_4^+, alkali ions like Rb^+ utilize perovskite structures.[12] The perovskite compounds often exhibit ferroelectric properties which is understood by spontaneous distortion of $\{BX_6\}$ and transition to a highly symmetrical cubic phase. They are attributed to the separation of the *d*-orbitals of the metal at the B-site for example Ti^{4+} in BTO. Thus, the reduction in symmetry in metal-free perovskites originates from another mechanism, for example the symmetry and ability to form hydrogen bonds of A-site molecule with

[a] *Graduate School of Sciences and Technology for Innovation, Yamaguchi University, Yoshida 1677-1, Yamaguchi, 753-8512, Japan.*
[b] *Institute of Multidisciplinary Research for Advanced Materials (IMRAM), Tohoku University, Sendai 980-8577, Japan*

Electronic Supplementary Information (ESI) available: details of experiment, XRD, TG-DTA, DSC, dielectric properties, and crystallographic consideration. See DOI: 10.1039/x0xx00000x

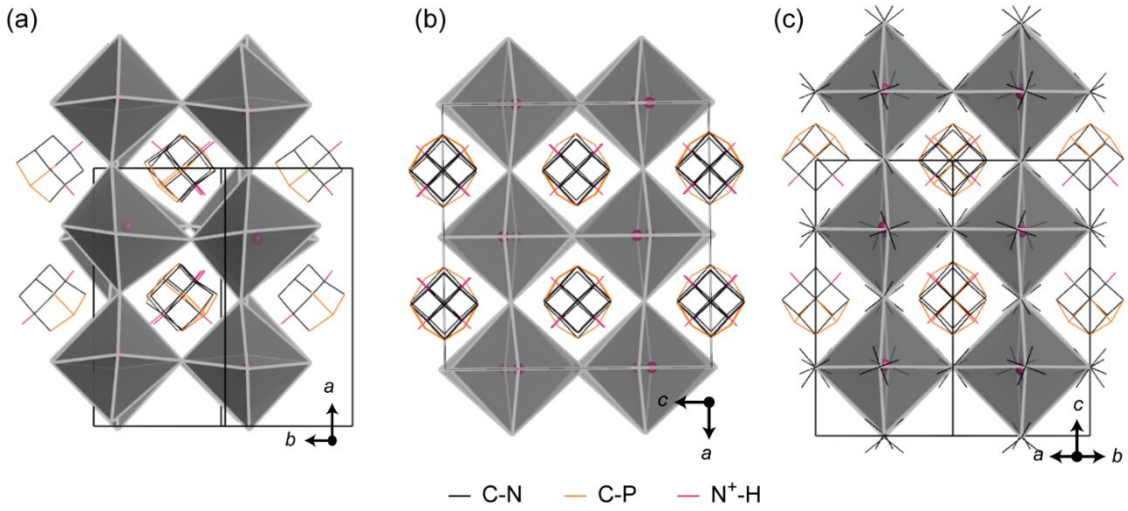

Figure 2. Crystal structure of (a) **p-Br**, (b) **p-I** and (c) **p-BF_4**. H atoms on C atoms were omitted.

the X anion. Not only ferroelectricity, a linear correlation was found between the band gap and the lowest unoccupied molecular orbital energies of the A^{2+} cations, indicating that the semiconducting properties are tailored through the molecular design of the A-site cation.[23]

The understanding and development of the metal-free perovskite family has been achieved through an investigation of the A-site cation and herein this study investigated 1,3,5-triaza-7-phosphaadamantane (pta) as a candidate for the A-site cation (Figure 1). This compound is a derivative of hmta where the P-atom has replaced the N-atom (Figure 1). The hmta is non-centrosymmetric and has been crystallised with a perovskite structures; $(H_2hmta)(NH_4)Br_3$ (**h-Br**)[26] and $(H_2hmta)(NH_4)(BF_4)_3$ (**h-BF_4**).[27] Three newly isolated metal-free perovskite crystals, represented by the formula $(H_2pta)(NH_4)X_3$ with X being Br^-, I^-, and BF_4^-, have been characterised in terms of their crystal structure, phase transition properties and photoluminescence.

Results and discussion

Synthetic procedures

Block crystals, which were colourless and of high quality, were isolated from an aqueous solution of pta and HX following evaporation in air. Compositions determined by CHN elemental analysis agreed with $(H_2pta)(NH_4)X_3$. Single crystal X-ray structure analysis (SC-XRD) at room temperature confirmed a quasi-cubic three-dimensional perovskite structure. Structural purities were validated from powder XRD analysis. Further details on crystallization and chemical and structural analyses were summarised in ESI.

Crystallographic studies

In the compound H_2pta^{2+}, two of the N-atoms were protonated as shown in Figure 1. The non-protonated nitrogen atom is distinguished by variations in the length of its C-N bond relative to the protonated nitrogen atom.[26] The C-N bond length in the protonated N of hmta is approximately 1.5 Å, which is greater than the bond length in the non-protonated form, which is less than 1.5 Å. Protonated nitrogen atoms were assigned based on this distinction.

For **p-Br**, a space group was classified as polar $Pna2_1$ at ambient temperature. In the **p-I** and **p-BF_4** crystals, A-site has static random disorder with the P- and N-atoms positioned with about a 50% crystallographic occupancy. However, two NH^+ were orientated towards specific direction in the crystals with polarisation anti-parallel, crystallising into centrosymmetric space group of the *Cmce* and $P4_2/n$ (Figure 2). Crystals of **p-Br** and **p-BF_4** are not isostructural with the hmta-based perovskites **h-Br** and **h-BF_4**. The larger P-atom in the pta molecule influences the orientation of molecules and symmetry of $\{NH_4X_6\}$ octahedra.

Table 1. Summary of structural data characterised by SC-XRD.

	p-Br	p-I	p-BF_4	h-Br	h-BF_4
T, K	251	251	251	253	252
V/*Z*, Å^3	328.3	363.6	394.2	309.8	376.1
V_{oct}, Å^3	54.3	60.1	65.5	51.6	62.4
D	0.0134 1	0.0050	0.0016	0.0160	0.0062
A, *deg*^{2}	147	134	19	165	50
t	0.949	0.933	0.928	0.912	0.892
μ	0.75	0.66	0.63	0.75	0.63
r_A, Å	2.63			2.45	
r_B, Å	1.46				
r_X, Å	1.96	2.20	2.32	1.96	2.32

Calculations of *D* and *A* were shown in ESI.

Structure and intermolecular interactions. The NH^+ groups on pta molecules interacted with X anions, resulting in a strong structural relationship between the orientation of H_2pta^{2+} and the distortion of $\{NH_4X_6\}$ octahedrons. The shortest distances between NH^+ of pta to Br^-or I^-were 3.308 Å (253 K) and 3.674 Å (253 K), respectively. They are longer than the mean values of $(CCC)N^+$–H···X (Br^- or I^-) distance of 3.247(7) Å and 3.50(3) Å,

indicating weak interaction.[28] Also, the distances between protonated N of H_2pta^{2+} and F atom in **p-BF₄** was 2.879 Å (233 K), comparable to weak interaction observed in NH_4BF_4 (2.914 Å).

Table 1 summarised certain crystallographic data of **p-X** and **h-X**. The volume of the lattice per formula unit (V/Z) and the volume of the octahedron (V_{oct}) both rose as the size of the X anion was large and as N (hmta) was substituted for P (pta). Distortion indexes (D) were calculated from the interatomic distances between the N-atom of the ammonium ion and the centre of the X anion (Br, I, and B atoms). The bond angle variance, denoted by (A, deg^2), was calculated for the octahedra. For regular octahedra, these values converge to zero. As the size of the anion grew, The D and A for **p-X** and **h-X** concurrently decreased, implying a correlation between the sizes of anion and the distortion of octahedral structures for metal-free perovskites with adamantane-type A-site cation.

Traditional tolerance factor. Perovskite structure is often predicted with tolerance factor t and octahedral factor μ. These values are given by

$$t = \frac{r_A + r_X}{\sqrt{2}\,(r_B + r_X)} \qquad \text{eq. 1}$$

$$\mu = \frac{r_B}{r_X} \qquad \text{eq. 2}$$

, r_A, r_B, and r_X are the radii of molecules and/or ions occupying A, B, and X sites, respectively. The parameter μ is a geometric requirement for octahedral {BX_6} structures. The quasi-cubic perovskite structures are expected for the cases of $0.813 < t < 1.107$ and $0.414 < \mu < 0.90$.[23, 30] The r_A, r_B and r_X were summarised in Table 1 with t and μ. However, it is difficult to determine the intrinsic radius of the A-site molecular cations. Thus, we estimate the radius as the distance between the centre of mass of the organic cation and the atom with the largest distance to it.[23] According to this estimation from SC-XRD data, radii were 2.63 Å and 2.45 Å for H_2pta^{2+} and H_2hmta^{2+}, respectively. The difference in radii is slightly smaller than that expected from the vdW radii of N (1.55 Å) and P (1.80 Å), 0.25 Å.

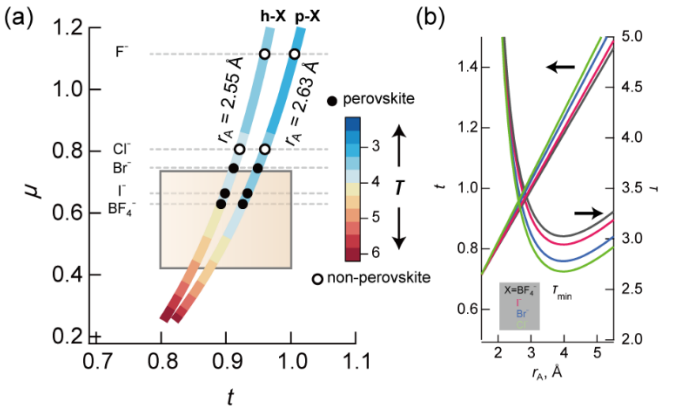

Figure 3. (a) Map of t and μ for **p-X** and **h-X** with coloured with τ (square represent area $0.8 < t < 1.0$ and $0.414 < \mu < 0.732$). (b) Plot of t and τ with r_A for different X (Cl^-, Br^-, I^- and BF_4^-).

The t values of **p-Br**, **p-I**, and **p-BF₄** were estimated to be 0.949, 0.933, and 0.928, respectively. Figure 3a shows a map of t and μ for **p-X** and **h-X**. The t values were within the range of prediction for the perovskite structure. The metal-free perovskite with Br^- salts were also reported for not only pta and hmta but also dabco and other compounds. However, quasi-cubic perovskite structures with Cl^- and F^- have not yet been isolated, except for the case in which water molecules are crystallised to occupy a space within the lattice.[8] The border of μ to maintain perovskite structure in **h-X** and **p-X** is between 0.75 (X=Br) and 0.81 (X=Cl).

Structure at t=1 corresponds to an ideal cubic perovskite structure with regular BX6 octahedra. In the structural model with r_A of 2.63 Å and 2.45 Å for H_2pta^{2+} and H_2hmta^{2+}, an ideal cubic structure is expected towards smaller anions X in the relationship between t and r_X in eq. 1. However, the experimental facts based on the values of D and A above show the opposite trend. Distrotion of octahedron increases with increasing anion size, indicating the limitation of a simple geometry model and/or contribution of the hydrogen bond in the lattice.

Consideration with new tolerance factor. Recently, Bartel et al. developed a new tolerance factor τ using an analytics approach which has the form

$$\tau = \mu^{-1} - n_A\left(n_A - \frac{r_A/r_B}{\ln\,(r_A/r_B)}\right) \qquad \text{eq. 3}$$

where n_A is the oxidation state of the A-site metal. The perovskite structure satisfied $\tau < 4.18$. The accuracy of the traditional tolerance factor by eq.1 is low for halide perovskites (chlorides 51%, bromides 56% and iodides 33%), but the consideration with the new tolerance factor resulted in high accuracy; chlorides 90%, bromides 93% and iodides 91% including organic-inorganic hybrids.[31] As τ decreases, the probability $P(\tau)$ for being perovskite increases from 0 to 1, where $P(\tau) = 0.5$ at $\tau = 0.418$. Perovskites with an inorganic-organic hybrid structure also meet this revised tolerance factor with a charge of organic cation as n_A.

The τ values for **p-X** and **h-X** were determined using a value of +2 for n_A, and a graph illustrating their relationships with μ and t is presented in Figure 3. Values below 4.18 indicate perovskite in blue, while values above 4.18 indicate non-perovskite in red (see also Table S7-1). Data for metal-free perovskites do not align with the τ-based assessment. As anion size decreases, τ-based probability rises, despite a lack of reported metal-free perovskites with F^- (this is also inconsistent with the t-μ plot analysis). Figure 3b is plots of t and τ against r_A for X=Cl^-, Br^-, I^- and BF_4^-. The τ has minimum value at $r_A/r_B = e$, *at* which r_A is calculated to 3.97 Å, however this is too large to form a perovskite structure, as expected from traditional tolerance factor t.

These mismatches with t and τ in **h-X** and **p-X** may be because there are fewer examples of metal-free perovskites reported than there are inorganic perovskites. The structural composition of $A^{2+}B^{+}(X^{-1})_3$, which is characteristic of metal-free perovskites, does not correspond to that of the metal-containing perovskites. For example, $BaNaBr_3$ is not a

perovskite and these compounds are treated as 'non-perovskites' in machine learning. The exploration of metal-free perovskites as a material group is still in its early stages, and further research is needed to develop successful analytic approaches that consider a wider range of materials with different A-site cations.

Temperature dependence of crystal structure

A peak was observed at 400 K in the DSC diagram of **p-Br**, suggesting a phase transition. The temperature-dependent SC-XRD analysis between 250 and 415 K determined the structure. A space group at high temperature phase was determined to *P*m-3m at which H_2pta^{2+} lost orientational order and $\{NH_4Br_6\}$ adopted the regular octahedron structure (Figure S2-2, Table S2-1). Changes in entropy and enthalpy for initial heating process were 4.46 kJ/mol and 10.6 J/mol K, respectively. These results suggest that phase change is an order-disorder type.

A plot in Figure 4 shows the unit cell volume per ABX_3 composition (*V*/*Z*) and normalised lattice parameters (see also Table S2-1). The crystal structure was determined to be orthorhombic at temperatures below 391 K. At temperatures above this point, the crystal structure well defined with a cubic system. At 391 K, R_{int} value is 0.1375 for orthorhombic system, higher than 0.0439 for cubic system (Figure S2-4).

The unit cell along the crystallographic *b*-direction decreases above 364 K, which corresponds to the contraction of its lattice volume. At 391 K, the lattice volume started to rise again. Similar negative thermal expansion was observed in perovskite compounds when the reduction of structural distortion from lower symmetry structure exceeded to degree of thermal expansion, for example, $PbTiO_3$.[32] Transition between polar and plastic crystalline phases is typical behaviour for ferroelectric crystals. The complex permittivity of **p-Br** was characterised between 120 and 370 K. Continuous increases in both real and imaginary parts were observed, indicating enhanced thermal motion in the crystal (Figure S5-1). However, no obvious electric field switching of spontaneous polarisation was observed using single crystals at 20.0 kV cm^{-1} and 1-100 Hz, where spherical hysteresis indicates the leakage current (Figure S5-2). In contrast to **p-Br**, no thermal anomalies which indicates phase transition to plastic crystal were observed for **p-I** and **p-BF_4**. This is because entropy change enough to phase transition was not gained from random disorder structure.

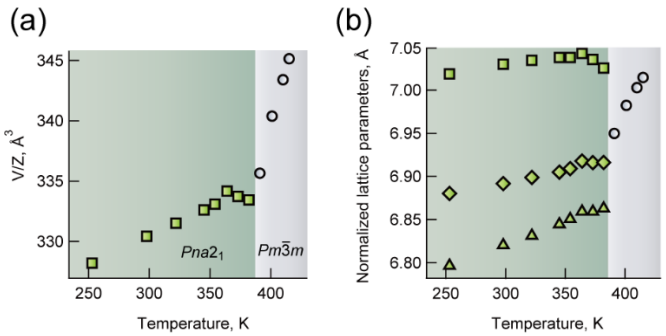

Figure 4. A plot of (a) *V*/*Z* and (b) normalised lattice parameters of **p-Br** (square=*b*, diamond=*a* and triangle=*c*) with temperature.

Compared to **h-Br** with **p-Br**, only the latter undergoes a phase transition to a plastic crystalline phase. Lattice entropies of both are considered to be comparable because P-atom does not form strong interaction, such as hydrogen bond, in the **p-Br**. Thus, there is two possible reasons; the larger size and lower symmetry of pta. Phase transition to the plastic crystalline phase is expected from larger lattice with weak interaction for **p-Br**. This is expected from larger *t* value of **p-Br**. The latter reason by symmetry resulted to high phase transition entropy of **p-Br**. In general for organic molecular solids, high symmetry molecules have higher melting points. This is because the number of possible states in the disordered liquid phase is reduced in a high symmetry molecule. Thus, the entropy changes in $T = \Delta H/\Delta S$ for melt goes small.[33] One approach to a quantitative estimation of the melting point is reported with entropy estimated by $R\ln(\sigma)$, where the σ depends on the point group of the molecule under consideration.

Compared to H_2hmta^{2+} (C_{2v}: σ=2) , which did not undergo a phase transition to the plastic crystalline phase, low symmetric H_2pta^{2+} (C_s: σ=1) is expected to lose orientational order at lower temperatures. The $R\ln(\sigma)$ estimated for H_2hmta^{2+} and H_2pta^{2+} are 5.76 and 0, respectively. With $\Delta H = T\Delta S$, the virtual phase transition temperature of **h-Br** can be estimated to ~920 K given if ΔH is identical to that of **p-Br**; $\Delta H/\Delta S = 4.46\times10^3/(10.6 - R\ln(2))$). This rough estimation agrees with the tendency of **h-Br** to decompose before the phase transition to the plastic crystalline phase. Further clear understanding of the relationship between molecular symmetry at the A-site and transition temperature to the plastic crystalline phase will lead to insight into the design of ferroelectric materials and plastic crystals.

Photoluminescence

Iodide of metal-free perovskite $A(NH_4)I_3$ showed PL, for example, A = MDABCO (**Med-I**) and methylated and protonated piperazine ($C_5N_2H_{14}^{2+}$) (**Mepi-I**).[ref] In addition to these iodides, a single crystal of **p-I** also showed PL. Figure 5shows the PL and photoluminescent excitation (PLE) spectra with a picture of the crystals under UV light. The intensities were represented by relative values, which were determined by the maximum peak intensity as a unit. The PL colour of **p-I** was greenish, which differed from the orangish PL colour of **Med-I** and **MePi-I**. In the PLE spectrum, the strongest peak was observed at 327 nm with a sub-peak at 360 nm and a shoulder around 380 nm. This corresponds well to the spectrum of **Med-I**, which shows two strong peaks at 314 and 334 nm with sub-peak at 360 nm and a shoulder at 375 nm. Also, the PLE spectrum of **p-I** quantitatively agrees with **MePi-I**, which showed a main peak at 307 nm. In the PL spectrum, a broad peak appeared at 550 nm, which was shifted from 610 nm (**Med-I**)[ref] and 572 nm (**MePi-I**)[ref], agreeing with the visual colour differences between greenish and orangish. However, the mechanism of PL and redshift of PL in **p-I** has not been fully clarified yet. The self-trapped excitons ref and/or the photo-induced reaction-ref are both considered.

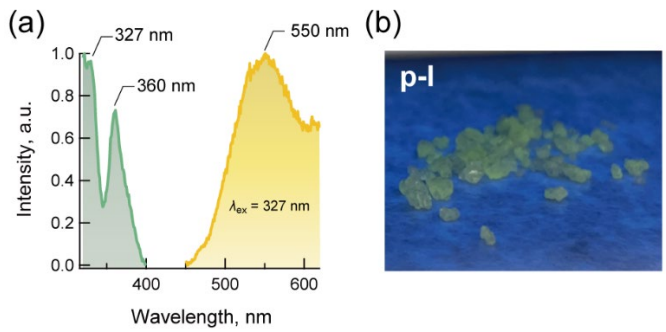

Figure 5. (a) PL and PLE (exited at 327 nm) spectra of p-H and (b) photograph of the single crystals **p-I** under UV light.

Conclusions

The development of a metal-free perovskite structure has been achieved through the investigation of organic cations which occupy the A-site in $A(NH_4)X_3$. Herein, metal-free perovskite structures containing phosphorus atoms, 1,3,5-triaza-7-phosphaadamantane (pta), were isolated with X = Br^-, I^-, and BF_4^-, and their structure and properties were studied. The bromide salt (**p-Br**) undergoes a phase transition involving the the orientational order-disorder of H_2pta^{2+}. In the **p-I** and **p-BF_4** crystals, the H_2pta^{2+} molecules exhibited random orientation, with their neutral nitrogen and phosphorus atoms in a state of disorder. The phase transition to the plastic crystalline phase observed for **p-Br** was attributed to the size and molecular symmetry of pta compared to hmta. A new tolerance factor obtained from machine learning of the inorganic metal-containing perovskite was employed to **p-X** and **h-X**; however, successful assignment was not obtained, indicating further discovery of the metal-free perovskite with variable A-site anion. In addition to other $A(NH_4)I_3$, the **p-I** also exhibited PL but a greenish colour, at room temperature. Introduction of P-atom at the A-site molecule led to differences in structure and phase transition compared with N-atom analogy in the adamantane-type A-site cation, revealing a new material design for metal-free perovskite.

Conflicts of interest

There are no conflicts to declare.

Acknowledgements

The acknowledgements come at the end of an article after the conclusions and before the notes and references.

Notes and references

1 A. S. Bain and P. Chand, *Ferroelectrics: Principles and Applications*, Wiley, 2017.
2 R. Waser, *Nanoelectronics and Information Technology: Advanced Electronic Materials and Novel Devices, 3rd Edition*, Wiley, 2012.
3 Q. Pan, Z. X. Gu, R. J. Zhou, Z. J. Feng, Y. A. Xiong, T. T. Sha, Y. M. You, R. G. Xiong, *Chem. Soc. Rev.* 2024, **53**, 5781–5861.
4 X. Song, G. Hodes, K. Zhao, S. Liu, *Adv. Energy Mater.* 2021, ***11***, DOI 10.1002/aenm.202003331.
5 Q. Cui, S. F. Liu, K. Zhao, *J. Phys. Chem. Lett.* 2022, **13**, 5168–5178.
6 R. Taheri-Ledari, F. Ganjali, S. Zarei-Shokat, M. Saeidirad, F. Ansari, M. Forouzandeh-Malati, F. Hassanzadeh-Afruzi, S. M. Hashemi, A. Maleki, *Energy and Fuels*, 2022, **36**, 10702–10720.
7 H. Y. Ye, Y. Y. Tang, P. F. Li, W. Q. Liao, J. X. Gao, X. N. Hua, H. Cai, P. P. Shi, Y. M. You, R. G. Xiong, *Science*, 2018, **361**, 151–155.
8 C. A. Bremner, M. Simpson, W. T. A. Harrison, *J. Am. Chem. Soc.*, 2002, **124**, 10960–10961.
9 M. Szafrański, *Cryst. Growth Des.*, 2018, **18**, 7106–7113.
10 S. L. Chen, Y. Shang, C. T. He, L. Y. Sun, Z. M. Ye, W. X. Zhang, X. M. Chen, *CrystEngComm*, 2018, **20**, 7458–7463.
11 L. Ye, Z. X. Gong, C. Shi, J. J. Ma, H. Liang, F. W. Qi, D. Y. E. Dian-Yu, C. F. Wang, Y. Zhang, H. Y. Ye, *CrystEngComm*, 2019, **21**, 7043–7047.
12 S. N. Cheng, K. Ding, T. Zhang, Z. X. Zhang, C. Y. Su, J. Z. Ge, Y. Zhang, D. W. Fu, *Chem. -Eur. J.*, 2021, **27**, 17655–17659.
13 H. Wang, H. Liu, Z. Zhang, Z. Liu, Z. Lv, T. Li, W. Ju, H. Li, X. Cai, H. Han, *npj Comput. Mater.*, 2019, ***5***, 1–9; H. S. Wu, B. T. Murti, J. Singh, P. K. Yang, M. L. Tsai, *Adv. Sci.*, 2022, **9**, 1–13.
14 X. Song, Q. Cui, Y. Liu, Z. Xu, H. Cohen, C. Ma, Y. Fan, Y. Zhang, H. Ye, Z. Peng, R. Li, Y. Chen, J. Wang, H. Sun, Z. Yang, Z. Liu, Z. Yang, W. Huang, G. Hodes, S. Liu, K. Zhao, *Adv. Mater.*, 2020, **32**, e202003353; X. Song, Q. Li, J. Han, C. Ma, Z. Xu, H. Li, P. Wang, Z. Yang, Q. Cui, L. Gao, Z. Quan, S. Liu, K. Zhao, *Adv. Mater.*, 2021, **33**, e202102190; Z. Li, G. Peng, H. Chen, C. Shi, Z. H. Li, Z. Jin, *Angew. Chem. Int. Ed*. 2022, **61**, e202207198.
15 M. G. Ehrenreich, Z. Zeng, S. Burger, M. R. Warren, M. W. Gaultois, J. C. Tan, G. Kieslich, *Chem. Commun.* 2019, **55**, 3911–3914.
16 L. C. An, K. Li, Z. G. Li, S. Zhu, Q. Li, Z. Z. Zhang, L. J. Ji, W. Li, X. H. Bu, *Small* 2021, **17**, 1–10.
17 R. Gao, X. Shi, J. Wang, G. Zhang, H. Huang, *Adv. Funct. Mater.* 2021, **31**, 1–11.
18 Y. Gao, S. Meshkat, A. Johnston, C. Zheng, G. Walters, Q. Feng, X. Wang, M. J. Sun, A. M. Najarian, D. Xue, Y. K. Wang, M. I. Saidaminov, O. Voznyy, S. Hoogland, E. H. Sargent, *ACS Appl. Mater. Interfaces* 2021, **13**, 19042–19047.
19 T. Handa, R. Hashimoto, G. Yumoto, T. Nakamura, A. Wakamiya, Y. Kanemitsu, *Sci. Adv.* 2022, **8**, eabo1621.
20 X. Song, Q. Li, J. Han, C. Ma, Z. Xu, H. Li, P. Wang, Z. Yang, Q. Cui, L. Gao, Z. Quan, S. Liu, K. Zhao, *Adv. Mater.* 2021, **33**, e202102190.
21 H. S. Choi, S. Li, I. H. Park, W. H. Liew, Z. Zhu, K. C. Kwon, L. Wang, I. H. Oh, S. Zheng, C. Su, Q. H. Xu, K. Yao, F. Pan, K. P. Loh, *Nat. Commun.* 2022, **13**, 6–12.
22 S. D. Gale, H. J. Lloyd, L. Male, M. R. Warren, L. K. Saunders, P. A. Anderson, H. H. M. Yeung, *CrystEngComm* 2022, **24**, 7272–7276.
23 J. Bie, D. B. Yang, M. G. Ju, Q. Pan, Y. M. You, W. Fa, X. C. Zeng, S. Chen, *JACS Au* 2021, **1**, 475–483.
24 H. Morita, R. Tsunashima, S. Nishihara, T. Akutagawa, *CrystEngComm* 2020, **22**, 2279–2282.
25 H. S. Choi, J. Lin, G. Wang, W. P. D. Wong, I. H. Park, F. Lin, J. Yin, K. Leng, J. Lin, K. P. Loh, *Science*, 2024, **384**, 60–66.
26 H. Morita, R. Tsunashima, S. Nishihara, K. Inoue, Y. Omura, Y. Suzuki, J. Kawamata, N. Hoshino, T. Akutagawa, *Angew. Chem. Ind. Ed.* 2019, **58**, 9184–9187.
27 J. Moriguchi, T. Koga, N. Tsunoji, S. Nishihara, T. Akutagawa, A. Masuya-Suzuki, R. Tsunashima, *Chem. Commun.* 2024, **60**, 12181–12184.
28 T. Steiner, *Acta Crystallogr. Sect. B Struct. Sci.* 1998, **54**, 456–463.

29 M. J. R. Clark, H. Lynton, *Can. J. Chem.* 1969, **47**, 2579–2586.
30 C. Li, X. Lu, W. Ding, L. Feng, Y. Gao, Z. Guo, *Acta Cryst. Sect. B Struct. Sci.* 2008, **64**, 702–707.
31 C. J. Bartel, C. Sutton, B. R. Goldsmith, R. Ouyang, C. B. Musgrave, L. M. Ghiringhelli, M. Scheffler, *Sci. Adv.* 2019, **5**, eaav0693.
32 R. J. D. Tilley, *Perovskites: Structure-Property Relationships, Wiley*, 2016, pp 281.
33 J. Wei, *Ind. Eng. Chem. Res*., 1999, **38**, 5019–5027.